DNA

MDPI

Article

The use of FLIM for characterising chromosomes and their structure in response to low-dose X-ray irradiation

Mohammed Yusuf1,4*, Sarah L. Berger2, Rosie Sanders2, Archana Bhartiya4, Rinyaporn Phengchat3, Robinson IK4, Stephen Barnard5, Benji Bateman2, Stanley W. Botchway2*

1 The Rosalind Franklin Institute, Rutherford Appleton Laboratory, Harwell Campus, Didcot, OX11 0QX
2 Central Laser Facility, UKRI- Science and Technology Facilities Council, Rutherford Appleton Laboratory, Harwell Science and Innovation Campus, Oxfordshire, OX11 0QX, U.K.
3 Quantum and Nanotechnology Research Centre, National Research Council Canada, 11421 Saskatchewan Drive, Edmonton, AB, T6G 2M9, Canada.
4 London Centre for Nanotechnology, University College London, London, WC1H 0AH, UK
5 UK Health Security Agency, Chilton, Oxfordshire OX11 0RQ
*Corresponding Authors: E-mail: Stan.Botchway@stfc.ac.uk; mohammed.yusuf@rfi.ac.uk
Shared First Authors.

Abstract

Chromosome research is essential for advancing our understanding of cytogenetics, gene regulation and numerous aspects of organismal health. It was demonstrated recently that staining chromosomes with 4',6-diamidino-2-phenylindole (DAPI) and applying Fluorescence Lifetime Imaging Microscopy (FLIM) enables the assessment of structural compaction changes in heterochromatin-rich region including chromosomes 1, with a shorter fluorescence lifetime (FLT) in the pericentromeric regions of this chromosome. We show that chromosome FLT was impacted by keeping the chromosomes hydrated whilst imaging. Following this, we used FLIM to optimise sample preparation conditions for more robust imaging and furthermore to measure the impact of low-dose ionising radiation on chromosome structure. We applied this method to different DNA stains bound to chromosomes where only DAPI led to a clear FLT difference between the arms with 2.98±0.12 ns and 2.65±0.07 ns on the pericentromeric region, while similar stains, such as Hoechst 33258 and NucBlue™ did not highlight these regions as clearly. While the FLT of chromosomes irradiated with 0.1 Gy and 1 Gy led to a slight increase in FLT, with 2.94±0.09 ns on the arms and 2.60±0.06 ns on the pericentromeric region of chromosome 1, 0.5 Gy led to a relevant reduction in FLT with 2.42±0.13 ns on the arms and 2.12±0.06 ns on the pericentromeric region of HeLa chromones. The same pattern could also be seen on X-ray irradiated T-cell chromosomes. These findings indicate that DAPI FLT may be a useful tool to measure chromosomal structural changes and further suggests that chromosomes undergo distinct structural changes following low-dose irradiation and are more sensitive to 0.5 Gy structural changes compared to the other doses tested.

Keywords: Chromosomes, DAPI, Fluorescence Lifetime Imaging Microscopy (FLIM), Multiphoton Microscopy, Confocal Imaging, T Cells, HeLa Cells, X-ray Irradiation, Ionising Radiation.

Academic Editor: Firstname Lastname

Received: date
Revised: date
Accepted: date
Published: date

Citation: To be added by editorial staff during production.

1. Introduction

Chromosomes serve as the fundamental units for storing and transmitting hereditary information, including genetic variation. Their preparation and analysis, particularly through karyotyping using Giemsa banding (G-banding), remain essential diagnostic tools in clinical medicine. This technique enables the detection of chromosomal instability and structural rearrangements, which are critical for diagnosing various haematological malignancies as well as prenatal and genetic disorders. These analyses are typically performed on metaphase chromosome "spreads," allowing for detailed visualisation of individual chromosomes and their banding patterns (Sumner, 1982; Tobias et al., 2011). Analysis of chromosome spreads offers critical insights into genome organisation and enables the investigation of various disease states, including chromosomal DNA damage.

Chromosomal DNA damage is a critical contributor to a range of pathological conditions, including genomic instability, mutagenesis, and oncogenesis. Such damage can arise from both endogenous and exogenous sources (Huang & Zhou, 2021). Endogenous damage is typically associated with cellular metabolic processes, including hydrolysis, oxidation, alkylation, and base mismatches. Exogenous damage, on the other hand, may result from exposure to non-ionising and ionising radiation such as ultraviolet (UV) light and various chemical agents. Direct interaction with DNA can lead to ionisation events that release electrons from atomic bonds, causing single- and double-strand breaks (Swarts et al., 2007). Fluorescence imaging remains a cornerstone in chromosome analysis and karyotyping. Furthermore, it is the most widely employed method for investigating chromosome organisation, structure and dynamics, offering high sensitivity and spatial resolution.

Excited-state lifetime measurements are a critical photophysical parameter that provides insights into the local molecular environment. These measurements can reveal information about molecular quenching (static or dynamic), pH, oxygen concentration, energy relaxation pathways, rotational dynamics, viscosity, and energy transfer processes (Jana et al., 2016; Botchway et al., 2008; Clancy et al., 2023; Ahmed et al., 2021). Fluorescence lifetime (FLT) refers to the average time a fluorophore remains in its excited state before emitting a photon and returning to the ground state. Fluorescence Lifetime Imaging Microscopy (FLIM) integrates these lifetime measurements with spatial fluorescence imaging, using either one-photon or multiphoton excitation. There are three principal methods for acquiring FLIM data: (1) frequency-domain lifetime measurements, (2) time-gated detection using sub-nanosecond gated cameras, and (3) time-correlated single photon counting (TCSPC) combined with scanning or widefield imaging systems (Botchway & Suhling, refs). In this study, we employed TCSPC-FLIM, which requires a pulsed excitation source (e.g., laser), a photon-sensitive detector with nanosecond resolution, and a precise timing system to synchronise photon arrival with the excitation pulse—ideally with picosecond accuracy (Botchway et al., 2021). FLIM thus offers a powerful approach for probing and visualising chromosomal environments at sub-micron resolution using intercalating chemical probes.

FLIM has emerged as a valuable tool for investigating the structural organisation and compaction state of mitotic chromosomes (Bhartiya et al, 2021; Botchway et al., 2021; Estandarte et al., 2016), representing a growing area of research in chromatin biology. According to Estandarte et al. (2016), FLIM of non-irradiated, fixed human metaphase chromosomes revealed shorter fluorescence lifetimes in chromosomes 1, 9, 15, 16, and Y, specifically in their heterochromatic rich regions, compared to the other chromosomes. These chromosomes are commonly referred to as heterochromatic due to the presence of distinct heterochromatin blocks near the pericentromeric regions. Pericentromeres are made up of repetitive tandem satellite repeats that are important for accurate chromosome segregation in mitosis (Saksouk et al, 2015). Constitutive heterochromatin is notably located at the pericentric regions of chromosomes 1, 9, and 16 (Tagarro, Fernández-Peralta, & González-Aguilera, 1994), the short p-arm of chromosome 15 (Friedrich et al., 1996; Chen et al., 1981), and the distal region of chromosome Y (Estandarte et al., 2016; Bachtrog, 2014; Choo, 1997; Meyne et al., 1984).

In this paper, first, we optimised sample preparation conditions for imaging chromosomes using FLIM. Once these conditions had been established, we investigated how X-ray irradiation at different doses (0.1 Gy, 0.5 Gy and 1 Gy) impacts chromosome FLT, mainly the heterochromatin rich pericentromeric region of the human genome. We show that the use of FLT is an excellent way to monitor the structural changes taking place during the imaging process.

2. Materials and Methods

Figure 1 presents a flowchart outlining the complete procedure for chromosome sample preparation and live cell X-ray irradiation.

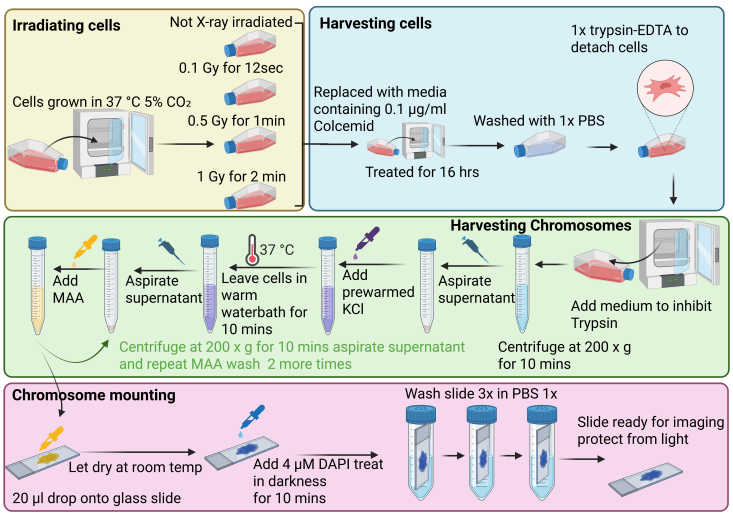

Figure 1. A Flow diagram showing chromosome preparation steps. Cells arex-ray irradiated using different doses (yellow box). Chromosomes are prepared after addition of Colcemid (mitotic

inhibitor); (blue box) followed by treatment with KCL (hypotonic) and then fixed using MAA (green box) before mounting onto glass slides (pink box). Created in Bio Render. Berger, S. (2025)

2.1. Cell culture

HeLa cells (Henrietta Lacks; human cervical cancer, passage 5) were cultured in T75 flasks using phenol red-free DMEM (Gibco, Life Technologies, UK), supplemented with 10% fetal bovine serum (FBS), 5 mM glutamine/1% GlutaMAX, and 1% penicillin-streptomycin (all from Gibco, Life Technologies, UK). Cultures were maintained at 37 °C in a humidified atmosphere with 5% CO_2. Chromosome preparations were performed when the cells reached 70–80% confluency.

Human T-cells, a primary cell line, were extracted from a female blood donor (provided by Dr. Sylwia Kabacik, UK Health and Security Agency). T-lymphocyte isolation and culture followed the protocol described by Bhartiya et al. (2021). Cells were incubated at 37 °C in a humidified 5% CO_2 environment, tilted at a 10° angle from horizontal. Once the culture reached a density of approximately 3×10^5 cells/mL, the cells were ready for X-ray irradiation and chromosome preparation.

2.2. X-ray Irradiation for Induction of Cellular DNA Damage

HeLa and human T-lymphocyte cells were irradiated with doses of 0.1 Gy (12 seconds), 0.5 Gy (1 minute), and 1 Gy (2 minutes), alongside a 0 Gy control, using hard X-rays at a dose rate of 1.7 Gy/min. Irradiation was conducted at the UK Health Security Agency (UKHSA, Harwell) under room temperature conditions. The X-ray source used was a 250 kVp, 13.0 mA unit operating at 500 mGy/min (AGO X-Ray Ltd., West Coker, UK), equipped with 1 mm copper and 1 mm aluminium filters to ensure beam quality and consistency.

2.3. Chromosome preparation and mounting on Microscope Glass Slides

Chromosomes were prepared using both previously established methods and an improved protocol (Bhartiya et al., 2021; Moralli et al., 2011; Yusuf et al., 2013; Berger et al., 2025). Once cell cultures reached the appropriate confluency, Colcemid (Thermo Fisher Scientific, UK) was added (0.1 μg/mL for HeLa cells, 0.2 μg/mL for T-cells), and cells were incubated for 16 hours at 37 °C in a humidified atmosphere with 5% CO_2. Following incubation, cells were harvested for chromosome preparation. Adherent cell lines (HeLa and HEK293) were detached by adding 3 mL of 1X trypsin-EDTA (Gibco, Life Technologies, UK) and incubating for 5 minutes at 37 °C. Detached cells were resuspended in 3 mL of culture medium and centrifuged at 200 x g for 10 minutes. The supernatant was discarded, and pre-warmed (37 °C) 75 mM potassium chloride (KCl; VWR, UK) was added dropwise to the pellet. Cells were incubated in a water bath at 37 °C for 10 minutes to induce hypotonic swelling, followed by centrifugation at 200 x g for 10 minutes. A freshly prepared 3:1 methanol (Scientific Laboratory Supplies, UK) and acetic acid (Sigma-Aldrich, UK) solution (MAA) was used for fixation. Fresh preparation is essential to prevent esterification and maintain effectiveness. After centrifugation, the supernatant was removed, and the MAA solution was added dropwise to the pellet while vortexing. The mixture was centrifuged again at 200 x g for 10 minutes. This MAA washing step was repeated three times. Fixed samples were stable for several months when stored at 4 °C.

20–30 μL of the fixed chromosome suspension was dropped onto the slide from a height of approximately 30 cm to ensure optimal spreading. This protocol was applied to all cell lines in the study except for human T-cells. For T-cell preparations, the suspension was dropped from a reduced height of approximately 5 cm above the slide to accommodate the different physical properties of the sample.

Before staining, all microscope slides were thoroughly dried. For DAPI staining, 15 μL of 4 μM DAPI (Thermo Fisher Scientific, UK) was applied to the centre of each slide. This concentration is optimal for FLIM applications (Estandarte, Bhartiya, Berger). A coverslip was then carefully placed over the drop to ensure even distribution of the stain across the entire coverslip area. The stained slides were incubated for 10 minutes, followed by a gentle wash with 1x PBS three times before imaging as indicated in Figure 1. A similar protocol was followed for other DNA stains: 15 μL of 4 μM Hoechst 33258 (Thermo Fisher Scientific, UK) and 1 drop of NucBlue™ (Thermo Fisher Scientific, UK) were applied to separate slides.

2.4. FLIM Acquisition and Data Analysis

Chromosome imaging was initially performed using wide-field epifluorescence microscopy to locate and assess chromosome spreads before confocal and FLIM acquisition. A Zeiss Z2 Axio Imager equipped with ISIS software was used to scan entire slides at 10× magnification, allowing the positions of chromosome spreads to be recorded. Higher magnification imaging was then performed using a 60× water immersion objective to focus on individual spreads, which were subsequently imaged using confocal microscopy with FLIM acquisition. The confocal-FLIM setup used in this study has been previously described (Estandarte et al.2016; Botchway et al., 2015). Briefly, single-photon excitation was achieved using a 405 nm and 410nm blue diode laser (Becker & Hickl). Imaging was conducted on a Nikon Ti-E or Ti2-E microscope equipped with a 60×, NA 1.2 water immersion objective. A Nikon EC2 confocal scan head was used to raster-scan the laser, and fluorescence was collected through the same objective. Detection was performed using a hybrid photomultiplier tube (HPM100-40, Becker & Hickl), with a 460/60 bandpass filter and an FL450 long-pass filter (Thorlabs) to eliminate laser scatter.

FLIM acquisition was carried out using the same confocal setup, integrated with a Becker & Hickl SPC830 or SPC-QC 104 time-correlated single-photon counting (TCSPC) module, controlled via SPCM software (version 9.0, 64-bit) (Figure 2). Images were acquired at a resolution of 256×256 or 512×512 pixels using FiFo mode, which records individual photon arrival times and spatial coordinates, storing the data on the TCSPC PC card. Before FLIM data acquisition, the instrument response function (IRF) was determined to correct for electronic noise and laser pulse fluctuations. Calibration was performed using fluorophores with well-characterised lifetimes, including 1 μM fluorescein, rhodamine B, and 7-hydroxycoumarin carboxylic acid in water. Imaging proceeded only when measured lifetimes were within 5% of published values (Ahmed et al., 2021).

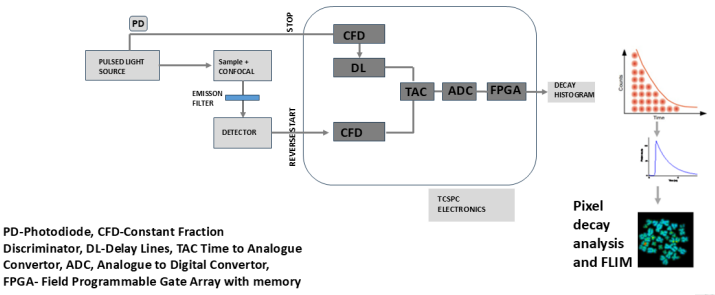

Figure 2. Schematic of FLIM measurement with a confocal laser scanning microscopy setup using sub-nanosecond excited state lifetime measurements using time-correlated single photon counting, TCSPC.

Following data acquisition, FLIM images were processed using SPCImage software version 8 (Becker & Hickl). The initial step in the analysis involved setting a photon count threshold to exclude pixels with insufficient signal. Typically, pixels with fewer than 25 and 35 photons per second in the peak channel were discarded, and 2-3 x binning was applied, depending on the background signal level, to ensure only pixels with adequate photon counts were analysed using Equation 1.

Typically, the threshold, low photon counts, is set to between 25 and 35 for the initial peak channel, with the exact threshold being determined by the level of the background signal. The main aim of this step is only to analyse pixels that have sufficient photon counts above the set threshold using equation 1. Next, the model for the exponential decay is set based on the decay curve shown, with the majority of FLIM readings requiring 'incomplete multiexponential' due to the long FLT, and a repetition rate time of 12.5 ns for the 80 MHz laser. When the laser repetition rate can be varied, this incomplete decay analysis is no longer necessary. Where an average count of 100 is lower than expected for most of the pixel binning, up to 3 times may be applied to increase the photon count for the analysis. We note that the xy pixel resolution of our confocal system is roughly 300 nm following excitation with 405 nm, and when a medium pinhole is applied. However, this has the effect of reducing the overall resolution of the FLIM image. The data points are fitted to a maximum-likelihood estimation model. The next parameter tested for is the chi-squared value, which needs to be between 0.9 – 1.3, as this is a measure of goodness of fit. Therefore, a chi-squared value of >1.3 suggests there are multiple lifetime components, whereas <0.8 may indicate a poor fit of the data. Both of which indicate that the data requires further and careful interpretation. The decay fitting for every pixel in the image generates a mean histogram lifetime distribution as well as individual distribution and FLT values for each pixel. A false-colour range may also be generated to allow comparison of different chromosome spreads.

Equation 1

$$I(t) = \sum_{i=1}^{n} \alpha_i \, exp\left(-\frac{t}{\tau_i}\right)$$

$$\tau_{ave} = \sum \alpha_i \tau_i$$

Moreover, R-studio was used to perform a Welch two-sample t-test comparing the different datasets obtained, and p-values of less than 0.05 were characterised as a significant difference in means between two samples.

3. Results

3.1. The effect of hydration and drying on DAPI FLT

To examine the effects of chromosome hydration on FLT, a HeLa chromosome spread was first imaged while kept wet in 1X PBS then left to dry at room temperature overnight and was reimaged the following day. FLTs on chromosome 1 arms and pericentromeric regions of wet and dry states were compared. Wet slides resulted with a FLT of 3.3±0.16 ns on the arms and 2.90±0.07 ns on the pericentromeric region of chromosome 1 (Figure 5Ai,ii,iii). However, the FLT of completely dry slides reduced to 2.05±0.06 ns on the arms and 1.84±0.06 ns on the pericentromeric region of chromosome 1. Drying led to a subtle FLT difference between pericentromeric regions and arms in addition to blurrier images due to a reduced DAPI signal (Figure 5Bi,ii,iii).

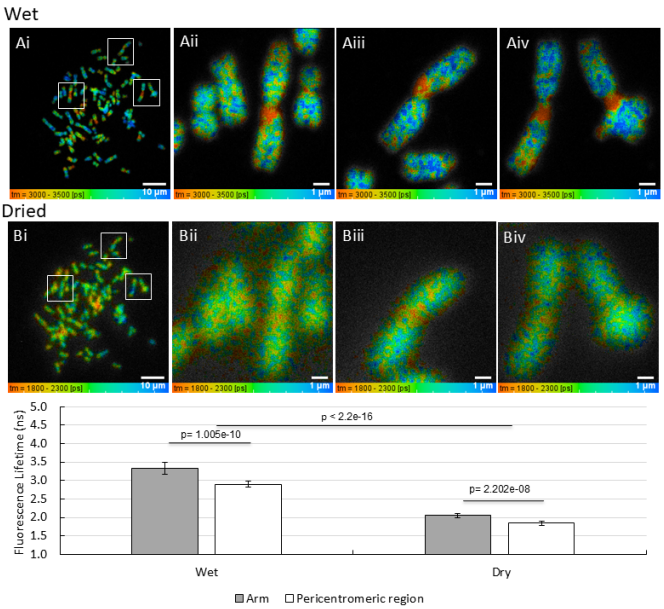

Figure 3. Importance of coverslip hydration and effect on chromosome fluorescence lifetime. The same HeLa chromosome spread stained with 4 μM DAPI is shown Ai,ii,iii) wet or Bi,ii,iii) dried. The graph indicates the pericentromeric region and the arm FLTs taken from 3 chromosome 1s, from the same spread, with 5 regions taken per centromere and per arm to calculate the average and standard deviations indicated in form or error bars, indicating a reduced lifetime and focus under dry conditions. P-values from a two-sample t-test compare the FLTs measured between pericentromeric and arm regions for each condition and the arm and pericentromeric

regions between the conditions with the first value representing the arm FLTs and the latter the pericentromeric FLTs. A 60x water objective was used.

3.2. *Effect of DAPI concentration on chromosome FLT*

Next, the effect of DAPI concentration was measured on HeLa chromosomes, to determine how the DAPI concentration affects that FLT under hydrated conditions. The HeLa chromosomes were prepared as described previously and stained with 4 μM, 40 μM and 400 μM of DAPI, then the FLT was measured as described in section 3.1. The results are shown in Figure 4 A, B and C, where a reduction in FLT is seen with increased concentration of DAPI from 4 μM with 3.30±0.10 ns on the arms and 2.87±0.07 ns on the pericentromeric region, to 40 μM with 2.76±0.09 ns on the arms and 2.41±0.07 ns on the pericentromeric region and 400 μM DAPI with 2.35±0.08 ns on the arms and 2.07±0.06 ns on the pericentromeric region of chromosome 1's (Figure 4).

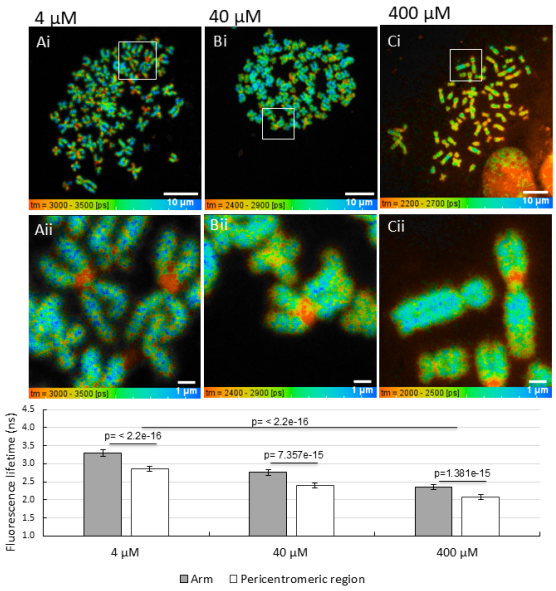

Figure 4. FLT comparisons between chromosomes stained with different DAPI concentrations. HeLa chromosomes were stained with Ai-ii) 4 μM, Bi-ii) 40 μM or Ci-ii) 400 μM. The graph highlights the pericentromeric region and arm FLTs of 5 chromosome 1s, from three different spreads, with 5 FLTs per pericentromeric region/arms to calculate the average and standard deviations shown as error bars. P-values from a two-sample t-test compare the FLTs measured between pericentromeric and arm regions for each condition and the arm and pericentromeric regions between the conditions with the first value representing the arm FLTs and the latter the pericentromeric FLTs. A 60x water objective was used.

3.3 *Investigating the sensitivity of different fluorescence stains for FLIM of chromosomes*

The FLT of three different DNA binding dyes Hoechst 33258 and DAPI and NucBlue™ (Hoechst 33342) and DAPI was compared. We compared the effectiveness of

these DNA stains to determine if there was any improvement in the experimental protocol compared to previously published work (Estandarte et al 2016) where chromosomes were not fully hydrated/not monitored. It was found that 4 μM Hoechst 33258 resulted in significant FLT difference between the chromosome arms 2.59±0.10 ns and the pericentromeric region 2.45±0.09 ns with a p-value of 0.001, as shown in in Figure 5A. Similarly, experiments were performed using one drop of NucBlue™ staining and also showed no significant difference between the arm of 3.43±0.13 ns to the pericentromeric region of 3.35±0.11 ns with a p-value of 0.208, as shown in Figure 5B. Changes were found for 4 μM DAPI-stained chromosomes showing a clear arm of 2.98±0.12 ns and a pericentromeric region of 2.65±0.07 ns FLT difference, as shown in Figure 5C.

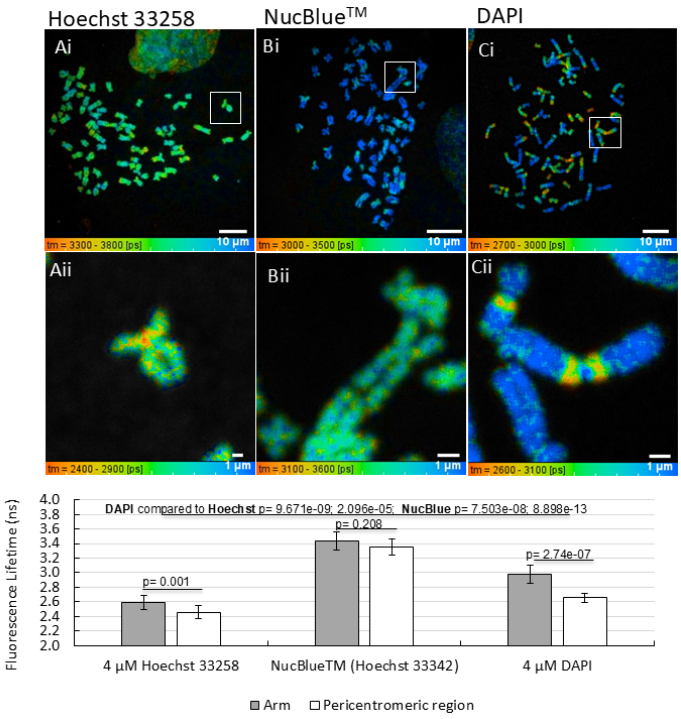

Figure 5. FLT comparison between different DNA staining dyes on HeLa chromosomes. Chromosomes were stained with Ai-ii) 4 μM Hoechst 33258, Bi-Bii) one drop of NucBlue™ and Ci-Cii) with 4 μM DAPI. The bar graph highlights the FLTs of 3 chromosome 1s from three different spreads, with 5 FLTs per arm/pericentromeric region to calculate the average and standard deviations shown as error bars. P-values from a two-sample t-test compare the FLTs measured between pericentromeric and arm regions for each condition and the arm and pericentromeric regions between the conditions with the first value representing the arm FLTs and the latter the pericentromeric FLTs. A 60x water objective was used.

3.4. Ionising radiation causes noticeable FLT changes in the pericentromeric and arm regions of chromosomes

Once the physical parameters and the optimisation process were established, we proceeded to test the effect of ionising irradiation on chromosomes using FLIM. After irradiating cells with a range of X-ray doses, 0.1, 0.5 and 1 Gy, chromosomes were prepared using the newly improved and optimised protocol as in section 3.1. At 0 Gy (control with no irradiation), a FLT of 2.94±0.09 ns on the arms and 2.60±0.06 ns on the pericentromeric region of chromosome 1 was measured, with a p-value of 8.227e-12 showing a significant difference between the mean FLTs between two regions (Figure 6A). At 0.1 Gy, both the arm and pericentromeric FLTs were increased slightly, to 3.08±0.10 ns (p-values of 0.0003) and 2.75±0.06 ns (p-values of 0.0002) on the arms and pericentromeric region, respectively (Figure 6B). Interestingly, when irradiation at 0.5 Gy led to a significant FLT reduction of 2.42±0.13 ns on the arms and 2.12±0.06 ns on the pericentromeric region (Figure 6C). Noteworthy, at 1 Gy, the FLTs increased to 3.05±0.13 ns on the arms and 2.67 ± 0.10 ns on the pericentromeric region with p-values of 0.01 on the arms and 0.06 on the pericentromeric region (Figure 6D). This 1 Gy FLT is similar to the FLT measured at 0 Gy. The difference in FLT between arms and pericentromeric region of chromosome 1 was seen in all conditions but presented with different p-values.

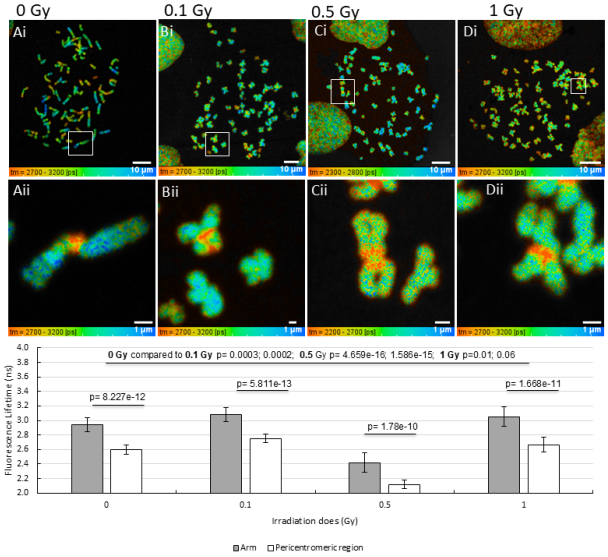

Figure 6. FLT comparison between chromosomes irradiated with different X-ray doses. FLT images of HeLa chromosomes stained with 4 µM DAPI that were Ai-ii) not irradiated, Bi-ii) irradiated with 0.1 Gy, Ci-ii) irradiated with 0.5 Gy or Di-ii) irradiated with 1 Gy. The clustered bar graph highlights these values, that have been obtained with by analyzing 4-5 chromosome 1s per condition, with 5 FLTs per arm and per pericentromeric area to generate average and standard deviations. P-values from a two-sample t-test compare the FLTs measured between pericentromeric and arm regions for each condition and the arm and pericentromeric regions between the conditions with the first value representing the arm FLTs and the latter the pericentromeric FLTs. A 60x water objective was used.

4. Discussion

In this study we established a suitable chromosome sample preparation condition for FLIM by keeping the sample hydrated. This allowed us to optimise the sample and imaging conditions further and allowed us to measure chromosome FLT in response to different X-ray irradiation doses. In this paper, we focussed specifically on chromosome 1, as it is the largest in the human genome and the easiest to identify and shows a difference between the chromosome arm and pericentromeric region.

A reduced DAPI fluorescence, when DAPI was in the dried environment, has been indicated previously by Barcellona et al. (1990), who explained that DAPI fluorescence is water dependent, as DAPI binding to the AT-rich minor groove releases solvation water molecules, which lead to an increase in fluorescence and quantum yield. Thus, when water is not present (such as the sample being in ethanol (Barcellona et al, 1990) or dried, it would lead to a lower fluorescence signal, as shown by the lower FLIM resolution due to lower photon counts in supplementary Figure 1. The FLTs of chromosomes measured using water or PBS 1X are supported by Ami et al. (2014), who found that pure water interacts with MAA and leads to chromosome structural changes. Moreover, PBS 1x is commonly used as a buffer for washing and maintaining samples and has also been used previously for washing and hydrating MAA chromosomes during imaging (Estandarte et al. (2016). Together, this highlights the importance of using PBS 1x for hydrating and washing chromosomes instead of using pure water (supplementary Figure 1). Moreover, the deterioration in image quality is not surprising since most high numerical aperture (>1) microscope objectives require an immersion medium such as water, oil or glycerol. The sample, therefore, needs to match this media. In our experiments, we have used a 60×, water NA 1.2 microscope objective. The photon counts will also be reduced since the refractive index of the sample and objective immersion (as well as the NA or angle of light collection from the sample by the objective) is reduced. The acquisition of good FLIM images relies on the level of photon count during the imaging process. Low photon counts require long acquisition times or higher than ideal laser powers, which may lead to sample photo-bleaching and damage. One source of low photon counts may be due to dry chromosome samples on the glass slide.

Therefore, in our experiments, we kept the slides hydrated by placing a drop of PBS 1X against the edge of the coverslip and allowing it to spread underneath until the entire surface area is covered (Figure 3). It is worth noting that this reduction in lifetime is not a consequence of the microscope NA but rather a good indication of the chromosome preparation quality and structural characteristics that are missing from the dried chromosome. This suggests that dried chromosomal DNA is somewhat different to that of a fully hydrated one. A significant decrease from the expected lifetime value indicates that chromosome drying up has a noticeable effect on the chromosome structure and is reported by the fluorescent properties of DAPI. This effect is generally ameliorated by rehydrating the sample. We also checked the effect of FLT of DAPI during MAA fixation drying (supplementary Figure 2) that gave a FLT reduction. This may be explained by considering the chemical properties of DAPI, which has two amidine functional groups, both can be involved in an alcohol and acids (Barcellona and Gratton, 1989) reaction. It is assumed that DAPI would react with the remaining MAA fixation solution and as a result, its fluorescent properties may change. Overall, our data indicates that FLT can be a simple way to determine the quality of chromosome preparation with FLIM. This is particularly important to ensure that any difference in FLT is reproducible and not influenced by large variations in sample preparation.

Once we established the method for FLIM of chromosomes whilst keeping the sample hydrated, we then measured the FLT of 3 different DAPI concentrations (4 μM, 40 μM and 400 μM). The use of DAPI for FLIM has been well established for chromosome imaging (Bhartiya et al, 2021; Botchway et al, 2021; Estandarte et al, 2016) where the hydration effect during imaging was not considered. It is a fluorescent stain that binds strongly to the DNA A-T minor groove (Tanious et al, 1992). Previously, Estandarte et al. (2016) measured the average FLT of chromosome 1s derived from GM18507 cells and showed no significant variations in DAPI FLT in response to concentration increase (0.4 μM, 4 μM, 40 μM and 400 μM). In this study, we enhanced our imaging by further measuring FLT on both the pericentromeric region of chromosome 1 and its arm for the 3 different DAPI concentrations (4 μM, 40 μM and 400 μM). We saw a significant reduction in DAPI FLT with increasing concentration from 4 to 400 uM (Figure 4). Why this reduction is occurring is unknown. We speculate it may be due to once of the following reasons i) that DAPI self-quenching may be occurring, leading to the reduction in FLT as the concentration increases ii) DAPI binds at a higher affinity to the pericentromeric region of chromosome 1 compared to its arms, leading to the reduced DAPI FLT on the pericentromeric region compared to the arms iii) this may be due to the difference in cell lines or sample preparation conditions (hydration vs no hydration).

We further validated our hydrated chromosome FLIM protocol by investigating the FLT of three different dyes, Hoechst 33258, DAPI and NucBlue™ (Hoechst 33342) that all bind to the minor groove of DNA and favour AT-rich regions (Cavatorta et al, 1985; Portugal and Waring, 1988; Chazotte et al, 2011). A further motivation for selecting these dyes was mainly due to the greater cell permeability by Hoechst (Breusegem et al, 2002), thus it is used mostly for live cell imaging. NucBlue™ labels the DNA in live cells faster than Hoechst 33258 and DAPI and has an excellent cell permeability. DAPI has shown to give a strong difference in FLT between the pericentromeric region and the arms of chromosome 1 but gave a shorter lifetime on chromosome 1 than the FLT measured in this study. Hoechst 33258 has previously shown a FLT difference (Estandarte et al, 2016). Whilst Hoechst 33258 was able to differentiate the arm and pericentromeric regions with asignificat value, the difference in FLT between pericentromeruic region and arms is less clear than DAPI. NucBlue™ was unable to provide much information on chromosome structure and environment since the lifetime values between the pericentromeric region and arms of chromosome 1, unlike with DAPI (Figure 3). Overall, our study suggests that DAPI is a better chromosome stain to use for detecting FLT changes in chromosomes than Hoechst 33258 and NucBlue™ under hydrated conditions.

Finally, we measured FLT of chromosomes in response to X-ray irradiation (Figure 6). The reason for the most significant change in FLTs measured at 0.5 Gy is unknown. Bhartiya et al (2021) showed in a X-ray Ptychography study that after irradiating T cells with different X-ray doses (0.1 Gy, 0.5 Gy and 1 Gy), the total mass of chromosomes at 0.1 Gy and 1 Gy was increased compared to the total mass of chromosomes at 0.5 Gy and was also reduced compared to 0 Gy (control). It is suggested that fewer proteins may be present on the chromosomes after irradiation dose of 0.5 Gy. At 0.1 Gy and 1 Gy proteins involved in the DNA damage response could be recruited to the chromosomes, thus increasing the total chromosome mass compared to 0 Gy. The recruitment of these proteins to the irradiated chromosomes may also be reflected in the FLT values in this study after irradiated HeLa and T-cell chromosomes (Figure 6), which show a FLT reduction at 0.5 Gy and a FLT increase at 0.1 Gy and 1 Gy compared to the non-irradiated

0 Gy chromosome on both the pericentromeric and arm regions of chromosome 1. A clear reduction in FLT at 0.5 Gy can only be found when the chromosomes are prepared, maintained and imaged with the newly established improved protocol keeping the coverslip hydrated (supplementary Figure 3A). Hence, our work suggests a need to continuously monitor the mounting slide throughout imaging, with coverslip hydration representing one of the first factors to check if unexpected lifetimes are being found.

The difference in FLTs in irradiated chromosomes may provide insight into the chromosomal structural changes, such as compaction status. Recruitment of the DNA damage repair protein to the DNA damaged sites could alter chromosome compaction as both DNA condensation and decompensation are part of the DNA Damage response pathway (Burgess et al., 2014). Additionally, Shimura and Kojima (2018) demonstrated that when exposing Human Umbilical Vein Endothelial Cells to 0.125 Gy, 0.25 Gy or 0.5 Gy X-ray irradiation, only at 0.5 Gy, an increase of γ-H2AX foci, an indication for DNA double-stranded breaks, can be observed compared to the 0 Gy non-irradiated cells. The studies above could explain the clear FLT response measured in HeLa and T-cells at 0.5 Gy compared to 0.1 Gy. However, the reason why the FLT of 1 Gy irradiated chromosomes is similar to that of the non-irradiated chromosome remain unknown.

While it is unclear why there is an increased sensitivity below 0.7 Gy for cell, it is interesting to note that we observe a difference in the lifetime of the percentromeric heterochromatin region at doses below 1 Gy. We therefore speculate that there may be a link between the hypersensitivity previously observed and what we observe in this study. Indeed, radiotherapy irradiations with 0.5 Gy fractions have been suggested as a more effective way of providing radiotherapy ultrafractionation (Lambin et al, 1993).

4. Conclusions

The importance of sample preparation in chromosome research is vital for medical and cell biological research. Here, we aimed to critically investigate and highlight experimental factors that influence the current chromosome preparation and imaging protocol, as well as a novel ionising radiation effect on the human pericentromeric region. We identified a number of optimisation procedures and applied them to human cell lines, focusing primarily on the following steps: fixation process, hydration, staining with DNA-binding probes, washing and imaging conditions. Although this study specifically focuses on the optimisation of chromosome sample preparation for the use in FLIM, this, in turn, informs on the quality of the chromosomes prepared. Using the FLIM technique together with the optimised process, we show that imaging of prepared chromosome slides should be ideally imaged immediately after staining, whilst the coverslips should be hydrated throughout the duration of imaging. Moreover, DAPI was found to be a more sensitive probe for FLIM for chromosome study than Hoechst and its derivatives. The technique improvements identified allowed determination of changes in chromosomes and the heterochromatin-rich pericentromeric region following ionising radiation, thus opening a new research direction for this difficult-to-study chromosome compaction and structure. We showed that irradiating live cells with ~0.5 Gy X-ray dose resulted in a change in the FLT at the pericentromeric region of chromosome 1, potentially indicating a damage-dependent chromosome compaction at this dose.

Future work

In this study, DAPI showed the largest difference between the pericentromeric region and arm of specific chromosomes, such as chromosome 1 in FLT of the stains investigated, suggesting that it might also be the most sensitive to other changes in the micro and nano-environment for future work involving chromosome imaging. It would be interesting to explore other pericentric heterochromatin rich chromosomes such as chromosome 9, 15, 16 and Y and apply mFISH assay for chromosome identification. Other DNA stains could be explored in order to improve FLIM sensitivity further. Moreover, in the future it would be interesting to explore the FLT on chromosomes after exposure of cells to other DNA-damaging agents, i.e ionising radiation sources such as UV and test environmental chemicals.

While this study focused on the impact of these optimisations of FLIM, many of the optimisations explored have potential for other microscopy techniques such as epifluorescence, confocal and super resolution. The latter, with a resolution of 10-100 nm, demands careful and excellent chromosome preparation techniques to determine the true structure.

Author Contributions:

Conceptualisation: Stanley W. Botchway, Ian Robinson and Mohammed Yusuf, Methodology: Sarah L. Berger, Rinyaporn Phengchat, Rosie Sanders, Stephen Barnard, Archana Bhartiya, Benji Bateman, Stanley W. Botchway and Mohammed Yusuf. Software: Sarah Berger, Rosie Sanders, Archana Bhartiya, Mohammed Yusuf, Stan W.Botchway. validation Sarah L. Berger, Rosie Sanders, , Archana Bhartiya, Stanley W. Botchway and Mohammed Yusuf. formal analysis, Sarah L. Berger, Rosie Sanders, , Archana Bhartiya, Stanley W. Botchway and Mohammed Yusuf; investigation: Stanley W. Botchway, Ian Robinson and Mohammed Yusuf, Methodology: Sarah L. Berger, Rinyaporn Phengchat, Rosie Sanders, Stephen Barnard, Archana Bhartiya, Benji Bateman, Stanley W. Botchway and Mohammed Yusuf. resources, Stan W Botchway and Mohammed Yusuf.; data curation, Sarah L. Berger, Rosie Sanders, , Archana Bhartiya, Stanley W. Botchway and Mohammed Yusuf. writing—original draft preparation, X.X.; Writing—original draft: Sarah L. Berger, Stanley W. Botchway, Mohammed Yusuf, Writing—review and editing: Sarah L. Berger, Rinyaporn Phengchat, Rosie Sanders, Archana Bhartiya, Stanley W. Botchway and Mohammed Yusuf, visualization, Sarah L. Berger, Rinyaporn Phengchat, Rosie Sanders, Archana Bhartiya, Stanley W. Botchway and Mohammed Yusuf; supervision, Stanley W. Botchway, Ian Robinson and Mohammed Yusuf ; project administration, Stanley W. Botchway, Ian Robinson and Mohammed Yusuf; funding acquisition Stanley W. Botchway, Ian Robinson and Mohammed Yusuf. All authors have read and agreed to the published version of the manuscript." Please turn to the CRediT taxonomy for the term explanation. Authorship must be limited to those who have contributed substantially to the work reported.

Funding: Please add: "This research received no external funding" or "This research was funded by NAME OF FUNDER, grant number XXX" and "The APC was funded by XXX". This work is supported by UKRI- STFC, funding access to the Central Laser Facility (SWB IM research). The Rosalind Franklin Institute is funded by the UK Research and Innovation, Engineering and Physical Sciences Research Council.

Institutional Review Board Statement: In this section, you should add the Institutional Review Board Statement and approval number, if relevant to your study. You might choose to exclude this statement if the study did not require ethical approval. Please note that the Editorial Office might ask you for further information. Please add "The study was conducted in accordance with the Declaration of Helsinki, and approved by the Institutional Review Board (or Ethics Committee) of NAME OF INSTITUTE (protocol code XXX and date of approval)." for studies involving humans. OR "The animal study protocol was approved by the Institutional Review Board (or Ethics Committee) of NAME OF INSTITUTE (protocol code XXX and date of approval)." for studies involving animals. OR "Ethical review and approval were waived for this study due to REASON (please provide a detailed justification)." OR "Not applicable" for studies not involving humans or animals.

Informed Consent Statement: Not applicable.

Data Availability Statement: We encourage all authors of articles published in MDPI journals to share their research data. In this section, please provide details regarding where data supporting reported results can be found, including links to publicly archived datasets analyzed or generated during the study. Where no new data were created, or where data is unavailable due to privacy or

ethical restrictions, a statement is still required. Suggested Data Availability Statements are available in section "MDPI Research Data Policies" at https://www.mdpi.com/ethics.

Acknowledgments: We are grateful to Dr Sylwia Kabacik, who performed the X-ray irradiations. The Rosalind Franklin Institute is funded by the UK Research and Innovation, Engineering and Physical Sciences Research Council. The authors have reviewed and edited the output and take full responsibility for the content of this publication.

Conflicts of Interest: The authors declare no conflicts of interest.

Appendix A

Appendix A.1

PBS 1X was chosen to hydrate the slide during washing and imaging, as pure deionised water led to significantly shorter FLT on the periphery of the chromosome spread as compared to the centre of the spread. Instead, when PBS 1X was used there was no FLT difference between the chromosome spread boarders and centre. Supplementary Figure 1 shows that pure deionised water led to significantly shorter FLTs on the chromosome spread periphery with a FLT 2.72±0.11 ns compared to the spread centre of 3.32±0.18 ns with a p-value of 1.747e-9. Instead, when PBS 1X was used to wash the chromosomes and were kept hydrated during imaging, both the chromosome spread periphery and the centre had no significant FLT difference between the. Thay had a p-value of 0.8 and an average FLT of 2.99 ± 0.09 ns throughout the spreads (3 spreads were analysed for each condition. While the FLTs differed significantly between the PBS 1X and water-maintained spreads, with a p-value of 6.798e-06 between centres and 4.144e-05 their peripheries (Supplementary Figure 1).

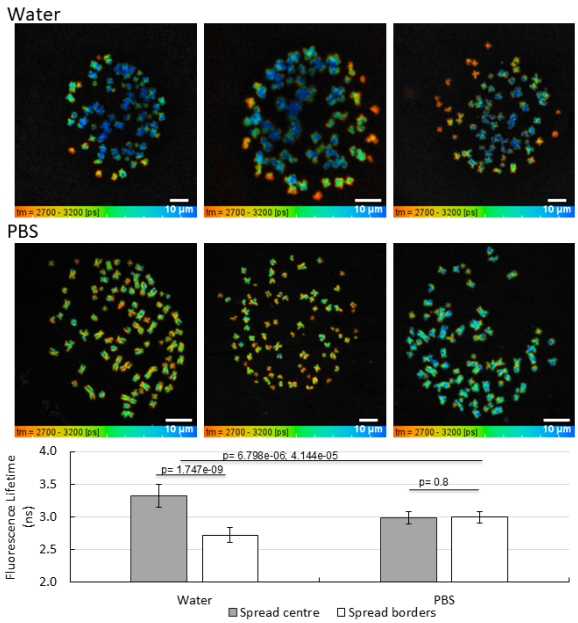

Supplementary Figure 1. FLT comparison between chromosomes hydrated with pure water or PBS 1X. FLT images of HeLa chromosome spreads stained with 4 µM DAPI and then either washed and hydrated with pure water or PBS 1X. The bar graph shows the average and standard deviation of three spreads per condition, in which 5 random FLTs were taken per centre/ border region. P-values from a two-sample t-test compare the FLTs measured between pericentromeric and arm regions for each condition and the arm and pericentromeric regions between the conditions with the first value representing the arm FLTs and the latter the pericentromeric FLTs. A 60x water objective was used.

Appendix A.2

As we preserved chromosomes using MAA, the FLT of HeLa chromosomes was measured in response to MAA drying time on a glass slide. Previously, the slides have always been allowed to dry completely before staining with 4 µM DAPI and then washed three times with PBS 1X. Here, an FLT comparison between completely dried MAA and wet MAA before adding DAPI was performed. Slides where the MAA was allowed to dry completely before adding DAPI led to a FLT of 3.0 ± 0.05 ns on the arms and 2.7 ± 0.06 ns on the pericentromeric regions of chromosome 1 (Supplementary Figure 2). However, when the MAA was not allowed to dry completely before staining with DAPI, no clear FLT difference between the pericentromeric region and arms could be seen with an FLT overall of 1.78 ± 0.04 ns. Here, the reaction with MAA results in a quenching of DAPI's fluorescent properties, leading to the observed lower FLT (Supplementary Figure 2).

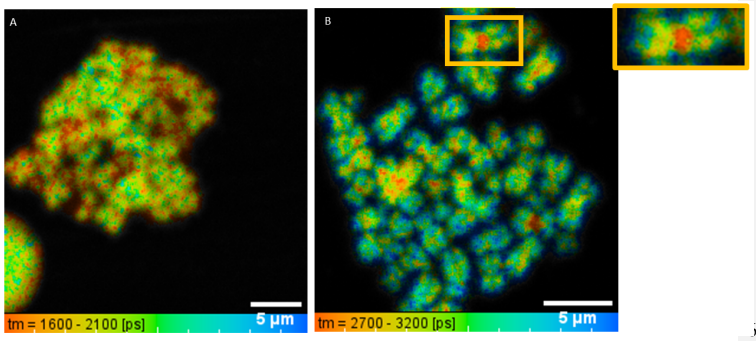

Supplementary Figure 2. The influence of MAA on chromosome FLT.
A T- cell chromosome spread was either A) wet or B) fully dried before staining the slide with 4 µM DAPI. A 60x water objective was used.

Appendix A.3

When comparing the FLTs of X-ray irradiated T-cells with the same doses as with the HeLa chromosomes, only the improved methods showed a clear FLT reduction with 0.5 Gy compared to the other doses (Supplementary Figure 3A). Whereas sub-optimal chromosome preparation conditions (likely due to improper drying of MAA, chromosome dehydration and lack of PBS 1X washing) led to a large variation in FLT, and a similar reduction in FLTs of arms and pericentromeric region for all irradiation doses compared to at 0 Gy (control with no irradiation) (Supplementary Figure 3B). In addition, at 0 Gy in the sub-optimal preparation, the significant difference in FLT between pericentromeric to arm FLTs was no longer observed (FLTs of 2.91 ± 0.09 ns on the arms and 2.81 ± 0.12 ns on the pericentromeric region, with a p-value of 0.09). In Supplementary Figure 3B the FLT difference between 0 Gy and 0.1 Gy is more significant, with 2.69 ± 0.08 ns on the arms and 2.59 ± 0.10 ns on the pericentromeric regions of chromosome 1 and p-values of 9.31e-9 and 5.328e-6 respectively and also a clear FLT difference between pericentromeric and arm regions at this does with a p-value of 7.902e-6. At 0.5 Gy, the FLT in Supplementary Figure 3A reduces significantly with p-values <2.2e-16 for both the arms and pericentromeric regions, with an arm FLT of 2.65 ± 0.06 ns and 2.40 ± 0.05 ns on the pericentromeric regions. On the other hand, in Supplementary Figure 3B, the pericentromeric to arm FLT difference at 0.5 Gy is not significant, with a p-value of 0.02 and 2.66 ± 0.11 ns on the arms and 2.55 ± 0.10 ns on the pericentromeric regions. While in Supplementary Figure 3B the difference between the FLTs measured with 0 Gy and 0.5 Gy is significant, with p-values of 6.731e-12 on the arms and 2.156e-7 on the pericentromeric regions, this difference becomes more significant in the improved protocol in Supplementary Figure 3A, with p-values <2.2e-16 for both the arms and pericentromeric regions.

For both Supplementary Figures 3A and B, an FLT increase from 0.5 Gy, which is similar to the one measured with 0 Gy, can be measured. However, the lifetimes increase more with the improved protocol, with an arm FLT of 2.92 ± 0.06 ns and a pericentromeric FLT of 2.70 ± 0.06 ns at 1Gy and p-values comparing the 0 Gy FLTs with the 1 Gy FLTs of 2.025e-5 and 0.001, respectively. This indicates that the pericentromeric regions of 0.1 Gy and 0 Gy are more similar to each other than their arm FLTs in Supplementary

Figure 4A. Instead, in Supplementary Figure 3B, the arm FLTs at 1 Gy are more similar to the arm FLTs at 0 Gy, with a p-value of 0.007 compared to the pericentromeric region FLTs with a p-value of 8.903e-5, with FLTs of 2.71 ± 0.12 ns on the 1 Gy arms and 2.61 ± 0.12 ns on the 1 Gy pericentromeric regions.

Commented [RP1]: This maybe can be removed as it's mentioned in the previous paragraph.

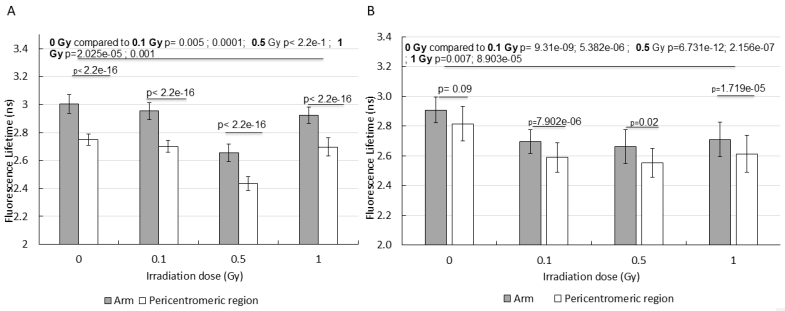

Supplementary Figure 3. DAPI FLT change of T cell chromosome 1s after different x-ray irradiation doses. A) Improved chromosome spread preparation (n=5) and B) dry sample preparation (chromosome spreads n = 9). The mean FLT in the arm and heteromorphic regions of cells irradiated with 0 Gy, 0.1 Gy, 0.5 Gy and 1 Gy is shown in the graphs. A 60x water objective was used for A and B. Grey bars show the FLT of the chromosome 1 arms whereas white bars show the FLT of the shorter heteromorphic regions of chromosome. Error bars represent standard deviation. For both graphs p-values from a two-sample t-test compare the FLTs measured between pericentromeric and arm regions for each condition and the arm and pericentromeric regions between the conditions with the first value representing the arm FLTs and the latter the pericentromeric FLTs.

References

Ahmed, A., Schoberer, J., Cooke, E., & Botchway, S. W. (2021). Multicolor FRET-FLIM Microscopy to Analyze Multiprotein Interactions in Live Cells. 287–301. https://doi.org/10.1007/978-1-0716-1126-5_16

Ami, D., di Segni, M., Forcella, M., Meraviglia, V., Baccarin, M., Doglia, S. M., & Terzoli, G. (2014). Role of water in chromosome spreading and swelling induced by acetic acid treatment: A FTIR spectroscopy study. European Journal of Histochemistry, 58(1), 33–39. https://doi.org/10.4081/ejh.2014.2330

Barcellona, M. L., & Gratton, E. (1989). Fluorescence lifetime distributions of DNA-4′,6-diamidino-2-phenylindole complex. Biochimica et Biophysica Acta (BBA) - General Subjects, 993(2–3), 174–178. https://doi.org/10.1016/0304-4165(89)90160-8

Barcellona, M. L., Cardiel, G., & Gratton, E. (1990). Time-resolved fluorescence of DAPI in solution and bound to polydeoxynucleotides. Biochemical and Biophysical Research Communications, 170(1), 270–280. https://doi.org/10.1016/0006-291X(90)91270-3

Bhartiya, A., Batey, D., Cipiccia, S., Shi, X., Rau, C., Botchway, S., Yusuf, M., & Robinson, I. K. (2021). X-ray Ptychography Imaging of Human Chromosomes After Low-dose Irradiation. Chromosome Research, 29(1), 107–126. https://doi.org/10.1007/s10577-021-09660-7

Binz, R. L., Burns, K., & Pathak, R. (2024). Protocol for preparation and staining of chromosomes isolated from mouse and human tissues for conventional and molecular cytogenetic analysis. STAR Protocols, 5(1), 102897. https://doi.org/10.1016/j.xpro.2024.102897

Botchway, S. W., Farooq, S., Sajid, A., Robinson, I. K., & Yusuf, M. (2021). Contribution of advanced fluorescence nano microscopy towards revealing mitotic chromosome structure. Chromosome Research. https://doi.org/10.1007/s10577-021-09654-5

Botchway, S. W., Parker, A. W., Bisby, R. H., & Crisostomo, A. G. (2008). Real-time cellular uptake of serotonin using fluorescence lifetime imaging with two-photon excitation. Microscopy Research and Technique, 71(4), 267–273. https://doi.org/10.1002/jemt.20548

Botchway, S. W., Scherer, K. M., Hook, S., Stubbs, C. D., Weston, E., Bisby, R. H., & Parker, A. W. (2015). A series of flexible design adaptations to the Nikon E-C1 and E-C2 confocal microscope systems for UV, multiphoton and FLIM imaging. Journal of Microscopy, 258(1), 68–78. https://doi.org/10.1111/jmi.12218

Breusegem, S. Y., Clegg, R. M., & Loontiens, F. G. (2002). Base-sequence specificity of Hoechst 33258 and DAPI binding to five (A/T)4 DNA sites with kinetic evidence for more than one high-affinity Hoechst 33258-AATT complex. Journal of Molecular Biology, 315(5), 1049–1061. https://doi.org/10.1006/jmbi.2001.5301

Burgess, Rebecca C., Burman, B., Kruhlak, Michael J. and Misteli, T. (2014). Activation of DNA Damage Response Signaling by Condensed Chromatin. Cell Reports, [online] 9(5), pp.1703–1717. doi:https://doi.org/10.1016/j.celrep.2014.10.060.

Cavatorta, P., Masotti, L., & Szabo, A. G. (1985). A time-resolved fluorescence study of 4′,6′-diamidine-2-phenylindole dihydrochloride binding to polynucleotides. Biophysical Chemistry, 22(1–2), 11–16. https://doi.org/10.1016/0301-4622(85)80021-1

Clancy, E., Ramadurai, S., Needham, S. R., Baker, K., Eastwood, T. A., Weinstein, J. A., Mulvihill, D. P., & Botchway, S. W. (2023). Fluorescence and phosphorescence lifetime imaging reveals a significant cell nuclear viscosity and refractive index changes upon DNA damage. Scientific Reports, 13(1), 422. https://doi.org/10.1038/s41598-022-26880-x

Durante, M. and Formenti, S.C. (2018). Radiation-Induced Chromosomal Aberrations and Immunotherapy: Micronuclei, Cytosolic DNA, and Interferon-Production Pathway. Frontiers in Oncology, [online] 8. doi:https://doi.org/10.3389/fonc.2018.00192.

Estandarte, A. K., Botchway, S., Lynch, C., Yusuf, M., & Robinson, I. (2016). The use of DAPI fluorescence lifetime imaging for investigating chromatin condensation in human chromosomes. Scientific Reports, 6(31417), 1–12. https://doi.org/10.1038/srep31417

Haraguchi, T., Kaneda, T., & Hiraoka, Y. (1997). Dynamics of chromosomes and microtubules visualized by multiple-wavelength fluorescence imaging in living mammalian cells: effects of mitotic inhibitors on cell cycle progression. Genes to Cells, 2(6), 369–380. https://doi.org/10.1046/j.1365-2443.1997.1280326.x

Hayashihara, K., Uchiyama, S., Kobayashi, S., Yanagisawa, M., Matsunaga, S., & Fukui, K. (2008). Isolation method for human metaphase chromosomes. Protocol Exchange. https://doi.org/10.1038/nprot.2008.166

HSU, T. C. (1952). MAMMALIAN CHROMOSOMES IN VITRO. Journal of Heredity, 43(4), 167–172. https://doi.org/10.1093/oxfordjournals.jhered.a106296

Huang, R., & Zhou, P.-K. (2021). DNA damage repair: historical perspectives, mechanistic pathways and clinical translation for targeted cancer therapy. Signal Transduction and Targeted Therapy, 6(1), 254. https://doi.org/10.1038/s41392-021-00648-7

Hughes, A. (1952). Some Effects of Abnormal Tonicity on Dividing Cells in Chick Tissue Cultures. Journal of Cell Science, S3-93(22), 207–219. https://doi.org/10.1242/jcs.s3-93.22.207

Hungerford, D. A. (1965). Leukocytes Cultured from Small Inocula of Whole Blood and the Preparation of Metaphase Chromosomes by Treatment with Hypotonic KCL. Stain Technology, 40(6), 333–338. https://doi.org/10.3109/10520296509116440

Jana, A., Crowston, B. J., Shewring, J. R., McKenzie, L. K., Bryant, H. E., Botchway, S. W., Ward, A. D., Amoroso, A. J., Baggaley, E., & Ward, M. D. (2016). Heteronuclear Ir(III)–Ln(III) Luminescent Complexes: Small-Molecule Probes for Dual Modal Imaging and Oxygen Sensing. Inorganic Chemistry, 55(11), 5623–5633. https://doi.org/10.1021/acs.inorgchem.6b00702

Joiner, M. C., Marples, B., Lambin, P., Short, S. C., & Turesson, I. (2001). Low-dose hypersensitivity: current status and possible mechanisms. International Journal of Radiation Oncology*Biology*Physics, 49(2), 379–389. https://doi.org/10.1016/S0360-3016(00)01471-1

Lambin P., Malaise E.P., & Joiner M.C. (1993). Megafractionnement: Une methode pour agir sur les tumeurs intrinsequement radio-resistantes? Bulletin Du Cancer. Radiothérapie, 80(4), 417–423.

Lewis, C. D., & Laemmli, U. K. (1982). Higher order metaphase chromosome structure: Evidence for metalloprotein interactions. Cell, 29(1), 171–181. https://doi.org/10.1016/0092-8674(82)90101-5

Llères, D., James, J., Swift, S., Norman, D. G., & Lamond, A. I. (2009). Quantitative analysis of chromatin compaction in living cells using FLIM–FRET. The Journal of Cell Biology, 187(4), 481–496. https://doi.org/10.1083/jcb.200907029

Makino, S., & Nishimura, I. (1952). Water-Pretreatment Squash Technic: A New and Simple Practical Method for the Chromosome Study of Animals. Stain Technology, 27(1), 1–7. https://doi.org/10.3109/10520295209105053

Moralli, D., Yusuf, M., Mandegar, M. A., Khoja, S., Monaco, Z. L., & Volpi, E. V. (2011). An Improved Technique for Chromosomal Analysis of Human ES and iPS Cells. Stem Cell Reviews and Reports, 7(2), 471–477. https://doi.org/10.1007/s12015-010-9224-4

Phengchat, R., Takata, H., Morii, K., Inada, N., Murakoshi, H., Uchiyama, S., & Fukui, K. (2016). Calcium ions function as a booster of chromosome condensation. Scientific Reports, 6(1), 38281. https://doi.org/10.1038/srep38281

Portugal, J., & Waring, M. J. (1988). Assignment of DNA binding sites for 4′,6-diamidine-2-phenylindole and bisbenzimide (Hoechst 33258). A comparative footprinting study. Biochimica et Biophysica Acta (BBA) - Gene Structure and Expression, 949(2), 158–168. https://doi.org/10.1016/0167-4781(88)90079-6

Rønne, M. (1990). Chromosome preparation and high resolution banding (review). In Vivo (Athens, Greece), 4(6), 337–365.

Saksouk N, Simboeck E, Déjardin J. Constitutive heterochromatin formation and transcription in mammals. Epigenetics Chromatin. 2015 Jan 15;8:3. doi: 10.1186/1756-8935-8-3. PMID: 25788984; PMCID: PMC4363358.

Shimura, N. and Kojima, S. (2018). The Lowest Radiation Dose Having Molecular Changes in the Living Body. Dose-Response, [online] 16(2). doi:https://doi.org/10.1177/1559325818777326.

Sumner, A. T. (1982). The nature and mechanisms of chromosome banding. Cancer Genetics and Cytogenetics, 6(1), 59–87. https://doi.org/10.1016/0165-4608(82)90022-X

Sumner, A. T., Evans, H. J., & Buckland, R. A. (1973). Mechanisms involved in the banding of chromosomes with quinacrine and Giemsa. Experimental Cell Research, 81(1), 214–222. https://doi.org/10.1016/0014-4827(73)90128-6

Takefumi SONE, Megumi IWANO, Shouhei KOBAYASHI, Takeshi ISHIHARA, Naoto HORI, Hideaki TAKATA, Tatsuo USHIKI, S. U. nad K. F. (2002). Changes in Chromosomal Surface Structure by Different Isolation Conditions. Arch. Histol. Cytol, 65 (5), 445–455. http://www2.kobe-u.ac.jp/~ohmido/Ohmido Lab/CL2003/pdf/03AHC_TS.pdf

Tanious, F. A., Veal, J. M., Buczak, H., Ratmeyer, L. S., & Wilson, W. D. (1992). DAPI (4′,6-diamidino-2-phenylindole) binds differently to DNA and RNA: minor-groove binding at AT sites and intercalation at AU sites. Biochemistry, 31(12), 3103–3112. https://doi.org/10.1021/bi00127a010

Therman, E. (1980). Structure of the Eukaryotic Chromosome and the Karyotype. In Human Chromosomes (pp. 11–23). Springer US. https://doi.org/10.1007/978-1-4684-0107-3_2

Tobias, E. S., Connor, M., & Ferguson-Smith, M. (2011). Essential Medical Genetics, Includes Desktop Edition. In John Wiley & Sons.

Visvanathan, A., Ahmed, K., Even-Faitelson, L., Lleres, D., Bazett-Jones, D. P., & Lamond, A. I. (2013). Modulation of Higher Order Chromatin Conformation in Mammalian Cell Nuclei Can Be Mediated by Polyamines and Divalent Cations. PLoS ONE, 8(6), e67689. https://doi.org/10.1371/journal.pone.0067689

Yusuf, M., Leung, K., Morris, K. J., & Volpi, E. V. (2013). Comprehensive cytogenomic profile of the in vitro neuronal model SH-SY5Y. Neurogenetics, 14(1), 63–70. https://doi.org/10.1007/s10048-012-0350-9

Yusuf, M., Parmar, N., Bhella, G. K., & Robinson, I. K. (2014). A simple filtration technique for obtaining purified human chromosomes in suspension. BioTechniques, 56(5), 257–261. https://doi.org/10.2144/000114168